Proceedings of the 17th World Congress
The International Federation of Automatic Control
Seoul, Korea, July 6-11, 2008

Robust Control of Resistive Wall Modes in Tokamak Plasmas using μ-synthesis ⋆

J. Dalessio, E. Schuster * D.A. Humphreys, M.L. Walker ** Y. In, and J.S. Kim ***

* *Lehigh University, Bethlehem, PA 18015, USA, (Tel: 610-758-5253; e-mail: schuster@lehigh.edu).*
** *General Atomics, San Diego, CA 92121, USA*
*** *FAR-TECH Inc., San Diego, CA 92121*

Abstract:
In this work, μ-synthesis is employed to stabilize a model of the resistive wall mode (RWM) instability in the DIII-D tokamak. The GA/Far-Tech DIII-D RWM model is used to derive a linear state space representation of the mode dynamics. The key term in the model characterizing the magnitude of the instability is the time-varying uncertain parameter c_{pp}, which is related to the RWM growth rate γ. Taking advantage of the structure of the state matrices, the model is reformulated into a robust control framework, with the growth rate of the RWM modeled as an uncertain parameter. A robust controller that stabilizes the system for a range of practical growth rates is proposed and tested through simulations.

1. INTRODUCTION

Nuclear fusion produces energy through fusing together the nuclei of two light hydrogen atom isotopes (e.g., deuterium and tritium). Such a process requires extreme temperatures to occur, since the nuclei need to overcome the Coulomb barrier (both nuclei carry positive charges) in order to fuse. The confinement of this high-temperature, ionized, hydrogen gas called plasma can be provided by a magnetic confinement device (e.g., a tokamak, which is in the shape of a torus).

One of the major non-axisymmetric instabilities in tokamaks is the resistive wall mode (RWM), a form of plasma kink instability whose growth rate is moderated by the influence of a resistive wall (Walker [2006]). This instability is present in sufficiently high pressure plasmas which causes the plasma to kink similar to that of a garden hose. In a kink mode, the entire plasma configuration deforms in a helically symmetric manner with an extremely fast growth time (a few microseconds) generating time-varying magnetic perturbations that induce eddy currents in the surrounding conductive structure. These induced currents, in turn, generate magnetic fields that oppose the plasma deformation slowing the overall growth rate of the instability (to a few milliseconds), which allows the use of feedback to control the RWM. If the surrounding structure were perfectly conductive at a critical distance from the plasma, the system would be stabilized by the mode-induced eddy currents, however the resistive losses cause a decay in the wall currents, which allow for growth in the mode amplitude. At present, research efforts focus on the stabilization of the $n = 1$ RWM(the plasma perturbation repeats only once as the toroidal angle varies from 0 to 2π) because this instability is usually the first to occur when pressure increases.

The GA/Far-Tech DIII-D RWM model replaces the spatial perturbation of the plasma with an equivalent perturbation of surface current on a spatially fixed plasma boundary and represents the resistive wall using an eigenmode approach (Fransson [2003], In [2006]). The spatial and current perturbations are equivalent in the sense that they both produce the same magnetic field perturbation. Observations from experiments show that the mode spatial structure remains unchanged. Based on the surface current representation of the mode, a state-space model of the plant can be derived from Faraday's Law, with states consisting only of the surrounding wall current and the external control coil currents. Since the plasma is represented as a single mode, and due to the mode spatial invariance, the state space model is parameterized with a scalar coupling coefficient c_{pp}, which is directly related to the growth rate γ of the mode.

Although the plasma surface deformation cannot be directly measured in real time, the magnitude and phase of the deformation can be diagnosed from measurements by a set of 22 magnetic field sensors composed of poloidal magnetic field probes and saddle loops, which measure radial flux. A set of 12 internal feedback control coils (I-coils) can then be used to return the plasma to its original axisymmetric shape. Fig. 1 shows the arrangement of coils and sensors. Using an estimator, the 22 outputs are reduced to 2 outputs that represent the RWM orthogonal components of the assumed $n = 1$ mode pattern. These 2 outputs can be combined to calculate the amplitude and toroidal phase of the mode (Edgell [2002]). In addition, a typical quartet configuration reduces the number of controllable inputs from 12 to 3 by locking the phase of the I-coils in sets of 4. The plant can be modeled then as a 3 input, 2 output system.

In the past years there have been many efforts on feedback stabilization of resistive wall modes in DIII-D (Garafalo [2001]-Okabayashi [2005]) as well as in other tokamaks, such as HBT-EP, NSTX, and ITER. Most of these efforts focused on designing empirically-tuned, non-model-based, *PD* (proportional-derivative) controllers. Nevertheless, there has been some work on the development of optimal controllers

⋆ This work was supported in part by a grant from the Commonwealth of Pennsylvania, Department of Community and Economic Development, through the Pennsylvania Infrastructure Technology Alliance (PITA), the NSF CAREER award program (ECCS-0645086), and DoE contract number DE-FC02-04ER54698.

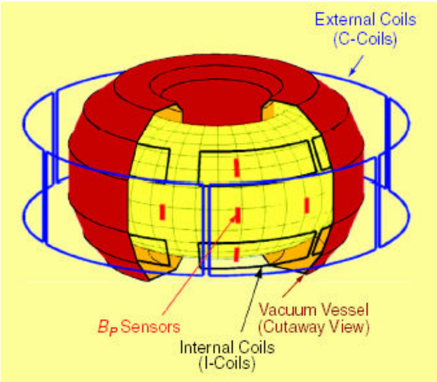

Fig. 1. Coils and sensors for magnetic feedback stabilization.

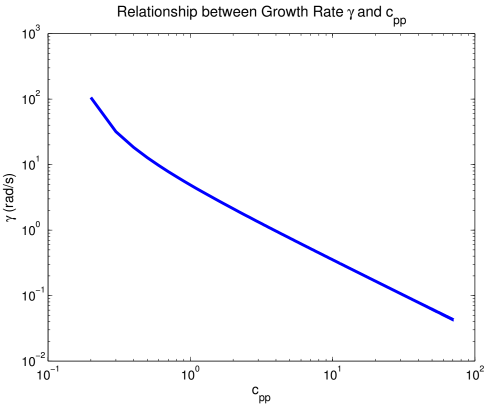

Fig. 2. Empirical relationship between growth rate γ and c_{pp}.

based on circuit models of the DIII-D tokamak (Sen [2003]) and ITER (Katsuro-Hopkins [2007]). Although some of these controllers have been proved effective in extending the stability region of the closed-loop system, they have been designed for a particular value of the system growth rate γ. The overall goal of this work is to take advantage of the developed DIII-D RWM model to design a model-based, feedback, stabilizing controller for a whole predefined range of the growth rate γ instead of a particular value (prior work in this direction can be found in (Sun [2006]), where an adaptive control approach is considered). The major parameter characterizing the magnitude of the instability is the time-varying uncertain parameter c_{pp}, which is related to the RWM growth rate γ . This parameter, in the form of the scalar coupling coefficient c_{pp}, is buried within the state space representation of the plasma and must be extracted and separated from the nominal plant model to write the model in a robust control framework. Once the uncertain parameter is extracted, a robust controller, as measured by the structured singular value μ (Zhou et al. [1996]), is designed to stabilize the RWM instability over a certain range of the growth rate γ. This has the benefits of designing one constant controller that can stabilize the plasma RWM instability over the entire physical range of the uncertain time-varying growth rate.

The paper is organized as follows. Section II introduces the GA/Far-Tech DIII-D RWM plasma model and manipulates the state space equation to achieve an affine parameterized form. Section III fully separates the uncertain parameter c_{pp} from the nominal plant using linear fractional transformations. Section IV describes the design of a robust controller based on the parameterized model using the $D-K$ iteration for μ-synthesis. The performance of the controller is assessed through simulations. Section V closes the paper stating the conclusions.

2. PLASMA MODEL & PARAMETERIZATION

2.1 System Model

Stated below is the GA/Far-Tech DIII-D RWM model, a plasma response model for the resistive wall mode using a toroidal current sheet to represent the plasma surface (Edgell [2002]). Most of the matrices and variables presented are characteristics of the tokamak and are well known. The uncertainty is introduced through the variable c_{pp}, which corresponds to a certain growth rate γ of the resistive wall mode. The relationship between these variables is shown empirically in Fig. 2 for a particular plasma equilibrium and is further explained in (In [2006]).

The model is represented in terms of the couplings between the plasma (p), vessel wall (w), and coils (c). The model derived from Faradays law of induction results in the system dynamics that reduce to

$$(M_{ss} - M_{sp}c_{pp}M_{ps})\dot{I}_s + R_{ss}I_s = V_s$$

where M_{ss} is the mutual inductance between external conductors, including the vessel wall and the coils, M_{sp} is the mutual inductance between either the external conductors and the plasma, R_{ss} is the resistance matrix, I_s is the current flowing in the conductors, and V_s is the externally applied voltage to the conductors. The mutual inductance matrices are given by

$$M_{ss} = \begin{bmatrix} M_{ww} & M_{wc} \\ M_{cw} & M_{cc} \end{bmatrix}, M_{sp} = \begin{bmatrix} M_{wp} \\ M_{cp} \end{bmatrix}, M_{ps} = [M_{pw} \;\; M_{pc}],$$

where M_{ps} and M_{sp} satisfy the following condition

$$M_{ps} = M_{sp}^T = \left[\, M_{wp}^T \;\; M_{cp}^T \,\right] \Rightarrow M_{pw} = M_{wp}^T, M_{pc} = M_{cp}^T.$$

The resistance matrix is given by

$$R_{ss} = \begin{bmatrix} \lambda_w & 0 \\ 0 & R_c \end{bmatrix},$$

where λ_w characterizes the couplings of a wall surface eigenmode to other states by the time-varying perpendicular magnetic fields contributed by those states and R_c is the coil resistance. The current and externally applied voltage to the conductors can be written as

$$I_s = \begin{bmatrix} I_w \\ I_c \end{bmatrix}, V_s = \begin{bmatrix} 0 \\ V_c \end{bmatrix},$$

where I_w is the wall current, I_c is the coil current, and V_c is the externally applied voltage to the coil.

This model can be represented in a state space formulation using the current in the conductors as the states ($x = I_s$) and the applied voltage as the inputs ($u = V_s$). This results in the following state space equation

$$\dot{x} = Ax + Bu$$

where

$$A = -L_{ss}^{-1}R_{ss}, \qquad B = L_{ss}^{-1}, \tag{1}$$

where $L_{ss} = M_{ss} - M_{sp}c_{pp}M_{ps}$. The output equation of the state space representation is based on sensor measurements that relate to the conductor currents through the dynamics

$$y = (C_{ss} - C_{yp}c_{pp}M_{ps})I_s$$

where C_{yp} is the coupling matrix between the sensor and plasma current and

$$C_{ss} = [\, C_{yw} \;\; C_{yc} \,]$$

is given by the coupling matrix between the sensor and wall current C_{yw}, and the coupling matrix between the sensor and coil current C_{yc}. This results in the state space output equation

$$y = Cx$$

where $C = C_{ss} - C_{yp}c_{pp}M_{ps}$.

2.2 Parameterization of the L_{ss}^{-1} Matrix

The goal of this section is to extract the uncertain parameter c_{pp} from the uncertain state space system and introduce it as an uncertainty block that perturbs a nominal state space system. The initial step to obtaining the nominal state space system is to express each state matrix as a general affine state space representation using nonlinear functions of the uncertainty c_{pp}. As seen in (1), the majority of the complexity is introduced in the A and B state matrices, where the uncertainty c_{pp} is introduced through L_{ss}^{-1}, and where $L_{ss} = (M_{ss} - M_{sp}c_{pp}M_{ps})$. Since the instability is two-dimensional, the matrix product $M_{sp}M_{ps}$ is rank 2 and the 2×2 diagonal C_{pp} matrix is treated as a scalar c_{pp}. Thus the L_{ss} matrix can be expressed as

$$L_{ss} = M_{ss} - M_{sp}c_{pp}M_{ps} = M_{ss} - c_{pp}\sum_{i=1}^{2} u_i u_i' \tag{2}$$

where $M_{sp} = M_{ps}' = [\, u_1 \;\; u_2 \,]$, and u_1 and u_2 are $n\times 1$ vectors where n is the number of states in the RWM state space model. To obtain a parameterized expression for the L_{ss}^{-1} term, we must first compute the inverse of a matrix sum. Given the matrix A_T, the scalar b_T, and the vectors C_T and D_T, the inverse of a matrix sum is given by the Sherman-Morrison formula as Kailath [1979]

$$(A_T - b_T C_T D_T)^{-1} = A_T^{-1} + \frac{b_T(A_T^{-1}C_T)(D_T A_T^{-1})}{1 - b_T D_T A_T^{-1} C_T}. \tag{3}$$

Using (2), the inverse of L_{ss} can be written as

$$L_{ss}^{-1} = (M_{ss} - M_{sp}c_{pp}M_{ps})^{-1} = (M_{ss} - c_{pp}u_1u_1' - c_{pp}u_2u_2')^{-1}.$$

Now, using the matrix $A_l = M_{ss} - c_{pp}u_1u_1'$ the above equation can be written as $L_{ss}^{-1} = (A_l - c_{pp}u_2u_2')^{-1}$. This is now in the form given by (3) and thus the formula can be applied, resulting in

$$L_{ss}^{-1} = A_l^{-1} + \frac{c_{pp}(A_l^{-1}u_2)(u_2'A_l^{-1})}{1 - c_{pp}u_2'A_l^{-1}u_2}. \tag{4}$$

Now the matrix L_{ss}^{-1} is expressed in terms of A_l^{-1}, which is equivalent to $(M_{ss} - c_{pp}u_1u_1')^{-1}$, and once again applying (3) results in

$$A_l^{-1} = (M_{ss} - c_{pp}u_1u_1')^{-1} = M_{ss}^{-1} + \frac{c_{pp}(M_{ss}^{-1}u_1)(u_1'M_{ss}^{-1})}{1 - c_{pp}u_1'M_{ss}^{-1}u_1}.$$

This expression can now be substituted back into (4). The terms can be collected and rewritten in the form

$$B = L_{ss}^{-1} = \sum_{i=0}^{4} \alpha_i B_i,$$

where α_i's are nonlinear functions of c_{pp}, and B_i's are constant matrices. The individual terms are given by

$$\alpha_0 = 1, \quad \alpha_1 = \frac{c_{pp}}{1 - c_{pp}u_1'M_{ss}^{-1}u_1}$$

$$\alpha_2 = \frac{c_{pp}}{1 - c_{pp}u_2'M_{ss}^{-1}u_2 - \frac{c_{pp}^2}{1 - c_{pp}u_1'M_{ss}^{-1}u_1}u_2'(M_{ss}^{-1}u_1)(u_1'M_{ss}^{-1})u_2}$$

$$\alpha_3 = \alpha_2\alpha_1, \quad \alpha_4 = \alpha_2\alpha_1^2, \quad B_0 = M_{ss}^{-1},$$

$$B_1 = [(M_{ss}^{-1}u_1)(u_1'M_{ss}^{-1})], \quad B_2 = \left[(M_{ss}^{-1}u_2)(u_2'M_{ss}^{-1})\right]$$

$$B_3 = \left[(M_{ss}^{-1}u_2)\left(u_2'(M_{ss}^{-1}u_1)(u_1'M_{ss}^{-1})\right) + \left((M_{ss}^{-1}u_1)(u_1'M_{ss}^{-1})u_2\right)\left(u_2'M_{ss}^{-1}\right)\right]$$

$$B_4 = \left[(M_{ss}^{-1}u_1)(u_1'M_{ss}^{-1})u_2u_2'(M_{ss}^{-1}u_1)(u_1'M_{ss}^{-1})\right].$$

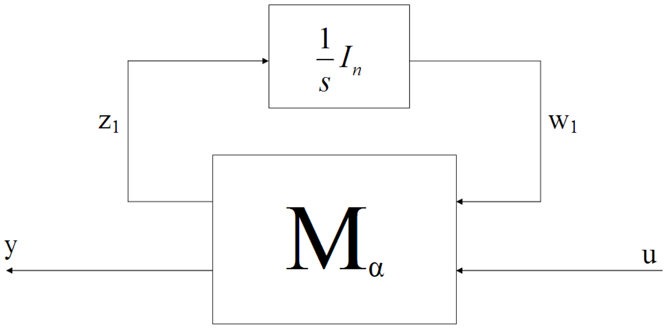

Fig. 3. $G(s)$ as a LFT using M_α, $\frac{1}{s}I_n$.

2.3 Expressing the Parameterized State Space Matrices

The last section allowed us to express the L_{ss}^{-1} matrix in a parameterized form, which allows the parameterization of the state and input matrices A and B respectively. In a similar way, the output matrix C can also be parameterized. Using the fact that c_{pp} is a scalar, the C matrix can be written as

$$C = C_{ss} - C_{yp}c_{pp}M_{ps} = C_{ss} - c_{pp}C_{yp}M_{ps} = C_0 + \alpha_5 C_5,$$

where

$$C_0 = C_{ss}, \quad C_5 = -C_{yp}M_{ps}, \quad \alpha_5 = c_{pp}.$$

Defining $A_i = -B_i R_{ss}$, we can finally summarize the parameterized expressions for the state matrices A, B, and C in terms of α_i's, given as

$$A = A_0 + \alpha_1 A_1 + \alpha_2 A_2 + \alpha_3 A_3 + \alpha_4 A_4 \tag{5}$$

$$B = B_0 + \alpha_1 B_1 + \alpha_2 B_2 + \alpha_3 B_3 + \alpha_4 B_4 \tag{6}$$

$$C = C_0 + \alpha_5 C_5. \tag{7}$$

3. GROWTH RATE PARAMETERIZATION

3.1 Linear Fractional Transformation (LFT) of RWM

A system with state space representation A,B,C,D has a transfer function $G(s) = D + C(sI_n - A)^{-1}B$, where n is the number of states (or eigenvalues) in the system and I_n is the convention used to describe an $n\times n$ identity matrix. Defining the matrix

$$M_\alpha = \begin{bmatrix} A & B \\ C & D \end{bmatrix}$$

we can write the transfer function as the linear fractional transformation of M_α as (Packard [1988])

$$\begin{aligned} G(s) &= F_u\left(\begin{bmatrix} A & B \\ C & D \end{bmatrix}, \frac{1}{s}I_n\right) = F_u\left(M_\alpha, \frac{1}{s}I_n\right) \\ &= M_{\alpha_{22}} + M_{\alpha_{21}}\frac{1}{s}I_n\left(I_n - M_{\alpha_{11}}\frac{1}{s}I_n\right)^{-1}M_{\alpha_{12}} \\ &= D + C\frac{1}{s}I_n\left(I_n - A\frac{1}{s}I_n\right)^{-1}B = D + C(sI_n - A)^{-1}B. \end{aligned}$$

The graphical representation of $G(s)$ is shown in Fig. 3, with equivalent equations

$$\begin{bmatrix} z_1 \\ y \end{bmatrix} = \begin{bmatrix} A & B \\ C & D \end{bmatrix}\begin{bmatrix} w_1 \\ u \end{bmatrix}$$

$$w_1 = \frac{1}{s}z_1, \quad y = F_u\left(M_\alpha, \frac{1}{s}I_n\right)u = G(s)u.$$

To introduce the uncertainty given by the parameterized state space system (5)-(7), the M_α matrix can be written in the form of a general affine state space uncertainty

$$M_\alpha = \begin{bmatrix} A_0 + \sum_{i=1}^{k} \alpha_i A_i & B_0 + \sum_{i=1}^{k} \alpha_i B_i \\ C_0 + \sum_{i=1}^{k} \alpha_i C_i & D_0 + \sum_{i=1}^{k} \alpha_i D_i \end{bmatrix}$$

with $k = 5, A_5 = 0, B_5 = 0, C_i = 0$ for $i = 1, \ldots, 4$, and $D_i = 0 \forall i$.

This uncertainty can be formulated into a linear fractional transform by achieving the smallest possible repeated blocks using the method outlined in (Packard [1988]). To begin this method, matrices J_i's are formed such that

$$J_i = \begin{bmatrix} A_i & B_i \\ C_i & D_i \end{bmatrix} \in \mathbb{R}^{(n+n_y)\times(n+n_u)}$$

for each $i = 1, \ldots, 5$. Then ,using singular value decomposition and grouping terms, an expression for J_i can be achieved (note: A^* is denoted as the complex conjugate transpose of A)

$$J_i = U_i \Sigma_i V_i^* = (U_i \sqrt{\Sigma_i})(\sqrt{\Sigma_i} V_i^*) = \begin{bmatrix} L_i \\ W_i \end{bmatrix} \begin{bmatrix} R_i \\ Z_i \end{bmatrix}^*.$$

Denoting q_i as the rank of each matrix J_i, each inner matrix is given by

$$L_i \in \mathbb{R}^{(n\times q_i)}, W_i \in \mathbb{R}^{(n_y\times q_i)}, R_i \in \mathbb{R}^{(n\times q_i)}, Z_i \in \mathbb{R}^{(n_u\times q_i)}.$$

Then, the uncertainty can be introduced as

$$\alpha_i J_i = \begin{bmatrix} L_i \\ W_i \end{bmatrix} [\alpha_i I_{q_i}] \begin{bmatrix} R_i \\ Z_i \end{bmatrix}^*,$$

where for this particular equilibrium, $q_1 = 1, q_2 = 1, q_3 = 2, q_4 = 1, q_5 = 2$. Finally, the linear fractional transformed matrix can be written as

$$M_\alpha = M_{11} + M_{12} \alpha_p M_{21},$$

where

$$M_{11} = \begin{bmatrix} A_0 & B_0 \\ C_0 & D_0 \end{bmatrix} \quad M_{12} = \begin{bmatrix} L_1 & \cdots & L_5 \\ W_1 & \cdots & W_5 \end{bmatrix}$$

$$M_{21} = \begin{bmatrix} R_1^* & Z_1^* \\ \vdots & \vdots \\ R_5^* & Z_5^* \end{bmatrix} \quad \alpha_p = \begin{bmatrix} \alpha_1 I_{q_1} & & 0 \\ & \ddots & \\ 0 & & \alpha_5 I_{q_5} \end{bmatrix}.$$

This is equivalent to the lower linear fractional transformation

$$M_\alpha = F_l(\begin{bmatrix} M_{11} & M_{12} \\ M_{21} & 0 \end{bmatrix}, \alpha_p) = F_l(M, \alpha_p)$$

$$= M_{11} + M_{12}\alpha_p (I_{q_T} - M_{22}\alpha_p)^{-1} M_{21} = M_{11} + M_{12}\alpha_p M_{21}$$

where

$$M = \begin{bmatrix} M_{11} & M_{12} \\ M_{21} & 0 \end{bmatrix},$$

and q_T is the total rank of the α_p matrix given by

$$q_T = \sum_i q_i = 7.$$

Finally, the transfer function of the uncertain state space model is written as

$$G(s) = F_u(M_\alpha, \frac{1}{s} I_n) = F_u(F_l(\begin{bmatrix} M_{11} & M_{12} \\ M_{21} & 0 \end{bmatrix}, \alpha_p), \frac{1}{s} I_n).$$

The graphical representation of G(s) is shown in Fig. 4 with the equivalent equations

$$\begin{bmatrix} \begin{bmatrix} z_1 \\ y \end{bmatrix} \\ z_2 \end{bmatrix} = \begin{bmatrix} M_{11} & M_{12} \\ M_{21} & 0 \end{bmatrix} \begin{bmatrix} \begin{bmatrix} w_1 \\ u \end{bmatrix} \\ w_2 \end{bmatrix}$$

$$w_1 = \frac{1}{s} z_1, \quad w_2 = \alpha_p z_2, \quad y = F_u(F_l(M, \alpha_p), \frac{1}{s} I_n) u = G(s) u.$$

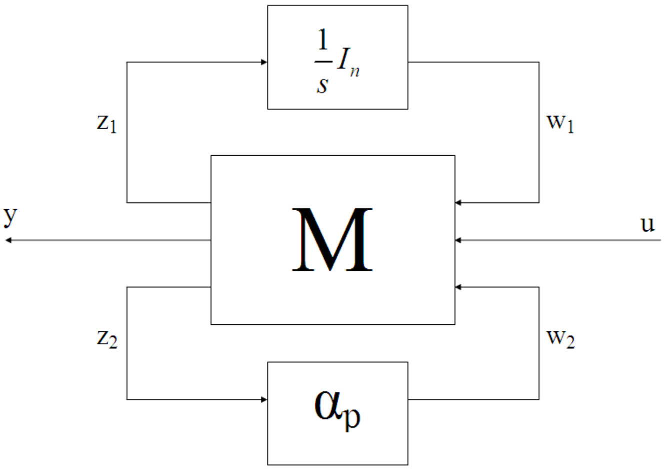

Fig. 4. G(s) as a LFT using M, α_p, $\frac{1}{s} I_n$.

3.2 Normalizing α Parameters

The system is now in a form where the uncertainty is given by the five α_i parameters. However, as shown earlier, each of the α_i parameters are nonlinear functions of the single variable c_{pp}. Thus the next step is to express the linear fractional transformation in terms of the single uncertainty c_{pp}. First, c_{pp} is normalized using

$$c_{pp} = d + \delta e,$$

$$d = c_{pp}^*, \quad e = max[|c_{pp_{max}} - c_{pp}^*|, |c_{pp_{min}} - c_{pp}^*|],$$

where c_{pp}^* is the nominal value of c_{pp}, and $c_{pp_{min}}$ and $c_{pp_{max}}$ are its minimum and maximum values respectively. This defines a new normalized uncertainty δ that has a range of values within $|\delta| \leq 1$ that corresponds to the desired c_{pp} range.

Now that each α_i parameter is expressed in terms of δ, we "pull out the δ" (Zhou et al. [1996]). This is done by drawing the block diagram for each α_i system and labeling the input to each δ block z_{3_i} and the output of each δ block w_{3_i}. Then the matrix Q, which satisfies $\alpha_p = F_l(Q, \Delta)$ with $\Delta = \delta I_{m_T}$, can be found using $\begin{bmatrix} w_{2_i} \\ z_{3_i} \end{bmatrix} \triangleq Q_i \begin{bmatrix} z_{2_i} \\ w_{3_i} \end{bmatrix}$ for each α_i term, where m_T is the total number of uncertainty elements needed to represent α_p. Thus the Q_i matrix satisfies the equation $\alpha_i = F_l(Q_i, \delta I_{m_i})$, where m_i is the minimum number of uncertainty elements δ needed to represent α_i. Recalling that $w_2 = \alpha_p z_2$, the system can be formulated such that $w_2 = F_l(Q, \Delta) z_2$. To correspond to each α_i term in the matrix α_p, the w_2, z_2, w_3, z_3 matrices are given by

$$w_2 = \begin{bmatrix} w_{2_1} \\ w_{2_2} \\ w_{2_3} \\ w_{2_4} \\ w_{2_5} \end{bmatrix}, z_2 = \begin{bmatrix} z_{2_1} \\ z_{2_2} \\ z_{2_3} \\ z_{2_4} \\ z_{2_5} \end{bmatrix}, w_3 = \begin{bmatrix} z_{3_1} \\ z_{3_2} \\ z_{3_3} \\ z_{3_4} \\ z_{3_5} \end{bmatrix}, z_3 = \begin{bmatrix} z_{3_1} \\ z_{3_2} \\ z_{3_3} \\ z_{3_4} \\ z_{3_5} \end{bmatrix},$$

where each w_{2_i} and z_{2_i} are vectors of length q_i, based on the rank of each J_i matrix, and each w_{3_i} and z_{3_i} are vectors of length $m_i q_i$, based on the minimum number of δ's required to represent each α_i and the value of q_i. The composite Q matrix will be defined after each individual Q_i is determined, where Q_i is given by $Q_i = \begin{bmatrix} Q_{i_{11}} & Q_{i_{12}} \\ Q_{i_{21}} & Q_{i_{22}} \end{bmatrix}$. The total number of uncertainty elements m_T for α_p is given by the total length of w_3, which is $m_T = \sum_i m_i q_i$. The block representation of α_p is show in Fig. 5.

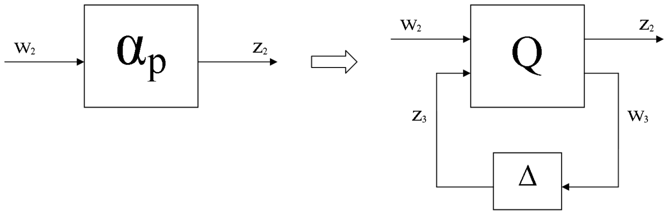

Fig. 5. α_p as a LFT using Q and Δ.

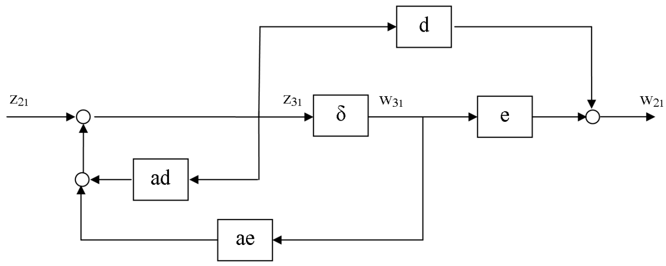

Fig. 6. Block Diagram for α_1.

Recalling that $\alpha_1 = \frac{c_{pp}}{1-c_{pp}u_1' M_{ss}^{-1} u_1}$, and using $a = u_1' M_{ss}^{-1} u_1$ and the normalized relationship $c_{pp} = d + \delta e$, we can rewrite $\alpha_1 = \frac{d+\delta e}{(1-ad)-ae\delta}$. Since there is only one uncertainty element, $m_1 = 1$. The block diagram for α_1, shown in Fig. 6, can be directly drawn from this form, with the feedback terms in the denominator and the feedforward terms in the numerator. Thus, the governing equation for α_1 is given by

$$\begin{bmatrix} w_{2_1} \\ z_{3_1} \end{bmatrix} = Q_1 \begin{bmatrix} z_{2_1} \\ w_{3_1} \end{bmatrix},$$

which results in a Q_1 given by

$$Q_1 = \begin{bmatrix} \dfrac{d}{1-ad} & e\left[1+\dfrac{ad}{1-ad}\right] \\ \dfrac{1}{1-ad} & \dfrac{ae}{1-ad} \end{bmatrix} = \begin{bmatrix} Q_{1_{11}} & Q_{1_{12}} \\ Q_{1_{21}} & Q_{1_{22}} \end{bmatrix}.$$

For the system matrices of the DIII-D tokamak under the particular equilibrium, the behavior of α_1 and α_2 are approximately the same, with an error on the order of 10^{-12}. From this very good approximation, we can take $\alpha_1 = \alpha_2$. Although the full model could be used, this is an accurate enough assumption that allows the reduction of computational complexity. As a result of this approximation, the following changes can be made to the other α parameters: $\alpha_3 = \alpha_2\alpha_1 \Rightarrow \alpha_3 = \alpha_1^2$, $\alpha_4 = \alpha_2\alpha_1^2 \Rightarrow \alpha_4 = \alpha_1^3$. Since $\alpha_2 = \alpha_1$, $m_2 = m_1 = 1$ and the Q_2 block is simply defined by $Q_2 = Q_1$. The parameter α_3 is given as $\alpha_3 = \alpha_1^2$, or $\alpha_3 = F_l(Q_1,\delta)\cdot F_l(Q_1,\delta)$. A reduction can be made so that $\alpha_3 = F_l(Q_3, \delta I_2)$, where I_2 is the size 2 identity matrix, thus $m_3 = 2$. Through the series connection of the linear fractional transform of Q_1, the Q_3 block is given by

$$Q_3 = \left[\begin{array}{c|cc} Q_{1_{11}}^2 & Q_{1_{11}}Q_{1_{12}} & Q_{1_{12}} \\ \hline Q_{1_{21}} & Q_{1_{22}} & 0 \\ Q_{1_{21}}Q_{1_{11}} & Q_{1_{21}}Q_{1_{12}} & Q_{1_{22}} \end{array}\right].$$

Similarly to Q_3, the parameter α_4 is given as $\alpha_4 = \alpha_1^3$, or $\alpha_4 = F_l(Q_1,\delta)\cdot F_l(Q_1,\delta)\cdot F_l(Q_1,\delta)$. A reduction can be made so that $\alpha_4 = F_l(Q_4, \delta I_3)$, where I_3 is the size 3 identity matrix, $m_4 = 3$, and Q_4 is given by the series connection of the linear fractional transform such that

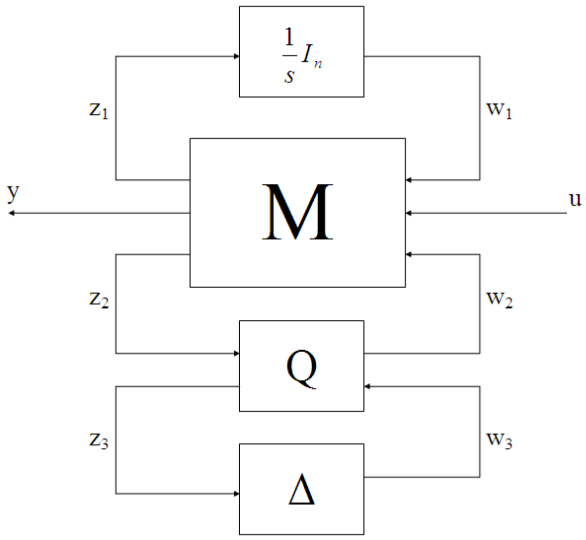

Fig. 7. G(s) as a LFT using M, Q, δ, $\frac{1}{s}I_n$.

$$Q_4 = \left[\begin{array}{c|ccc} Q_{1_{11}}^3 & Q_{1_{11}}^2 Q_{1_{12}} & Q_{1_{11}}Q_{1_{12}} & Q_{1_{12}} \\ \hline Q_{1_{21}} & Q_{1_{22}} & 0 & 0 \\ Q_{1_{21}}Q_{1_{11}} & Q_{1_{21}}Q_{1_{12}} & Q_{1_{22}} & 0 \\ Q_{1_{21}}Q_{1_{11}}^2 & Q_{1_{21}}Q_{1_{11}}Q_{1_{12}} & Q_{1_{21}}Q_{1_{12}} & Q_{1_{22}} \end{array}\right].$$

Also, Q_5 can be directly written as

$$Q_5 = \begin{bmatrix} d & e \\ 1 & 0 \end{bmatrix},$$

such that $m_5 = 1$.

Now that there is an expression for each of the α_i $(i = 1,\ldots,5)$ parameters in terms of a linear fractional transformation $\alpha_i = F_l(Q_i, \delta I_{m_i})$, they can be combined to form one linear fraction transformation with a common uncertainty δ. As shown earlier, the uncertainty in terms of α is given as

$$\alpha_p = \begin{bmatrix} \alpha_1 I_{q_1} & & & & 0 \\ & \alpha_2 I_{q_2} & & & \\ & & \alpha_3 I_{q_3} & & \\ & & & \alpha_4 I_{q_4} & \\ 0 & & & & \alpha_5 I_{q_5} \end{bmatrix},$$

where I_{q_i} is the size q_i identity matrix. The total number of uncertain elements is given by $m_T = \sum_i m_i q_i = 11$. Thus, the linear fractional transformation $\alpha_p = F_l(Q,\Delta)$ with $\Delta = \delta I_{m_T}$ is given by $\alpha_p = Q_{11} + Q_{12}\Delta(I_{m_T} - Q_{22}\Delta)^{-1}Q_{21}$ where $Q = \begin{bmatrix} Q_{11} & Q_{12} \\ Q_{21} & Q_{22} \end{bmatrix}$. Each submatrix Q_{jk} is given by the block diagonal matrix

$$Q_{jk} = \begin{bmatrix} Q_{1_{jk}} & & 0 \\ & \ddots & \\ 0 & & Q_{5_{jk}} \end{bmatrix}$$

where $j = 1,2$ and $k = 1,2$. The matrix Q_{jk} has the same number of diagonal blocks as α_p based on the rank of each J_i matrix denoted by q_i.

3.3 Model in Robust Control Framework

The final expanded representation of entire system is $G(s) = F_u(F_l(M, F_l(Q,\Delta)), \frac{1}{s}I_n)$, which is described by Fig. 7 and corresponding equation set

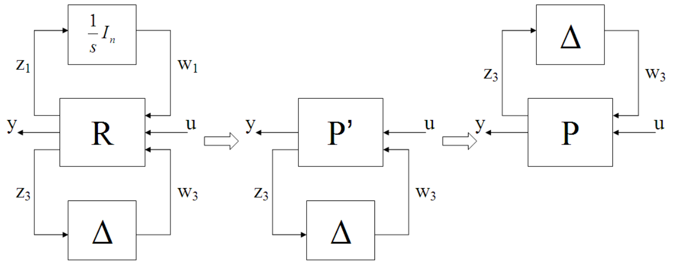

Fig. 8. Graphical representation of $G(s)$ manipulation.

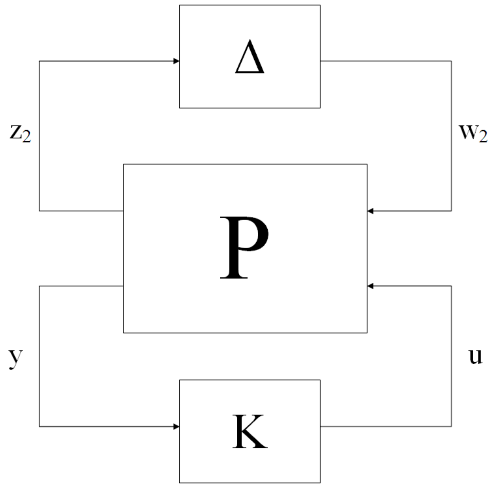

Fig. 9. General framework for robust control.

$$\begin{bmatrix} \begin{bmatrix} z_1 \\ y \end{bmatrix} \\ z_2 \end{bmatrix} = \begin{bmatrix} M_{11} & M_{12} \\ M_{21} & 0 \end{bmatrix} \begin{bmatrix} \begin{bmatrix} w_1 \\ u \end{bmatrix} \\ w_2 \end{bmatrix}$$

$$\begin{bmatrix} w_2 \\ z_3 \end{bmatrix} = \begin{bmatrix} Q_{11} & Q_{12} \\ Q_{21} & Q_{22} \end{bmatrix} \begin{bmatrix} z_2 \\ w_3 \end{bmatrix}$$

$$w_1 = \frac{1}{s} z_1,\, w_3 = \delta z_3,\, y = F_u(F_l(M, F_l(Q,\Delta)), \frac{1}{s} I_n) u = G(s)u.$$

Finally, the original system M can be combined with the matrix Q through the interconnection of LFT's Skogestad [2005]. This is done using the fact that $M_\alpha = F_l(M,\alpha_p) = F_l(M, F_l(Q,\Delta)) = F_l(R,\Delta)$ where R is equal to

$$R = \begin{bmatrix} M_{11} + M_{12}Q_{11}M_{21} & M_{12}Q_{12} \\ Q_{21}M_{21} & Q_{22} \end{bmatrix}.$$

Now the system is reduced to a simple form of R, uncertainty $\Delta = \delta I_{m_T}$ with $|\delta| \leq 1$, and $\frac{1}{s} I_n$. The system can now be reduced using a simple property of the LFT. The system given by $G(s) = F_u(F_l(R,\Delta), \frac{1}{s} I_n)$ can be written as $G(s) = F_l(F_u(R, \frac{1}{s} I_n), \Delta) = F_l(P',\Delta)$ where $P' = F_u(R, \frac{1}{s} I_n)$. The final step in the system reduction moves the uncertainty, creating an upper LFT for convention purposes. This is done by using $G(s) = F_l(P',\Delta) = F_u(P,\Delta)$ The overall system reduction is shown in Fig. 8.

The parameterization of the RWM model allows this system to be represented in the general framework of robust control for uncertain systems. The goal is to design a controller K that stabilizes the plant for all uncertainty $|\delta| \leq 1$. The feedback controller K can be applied to the plant to formulate a closed-loop LFT system on the uncertainty and the controller (Fig. 9)

$$G(s) = F_l(F_u(P,\Delta), K) = F_u(F_l(P,K), \Delta).$$

4. CONTROLLER SYNTHESIS AND SIMULATION

4.1 DK-iteration Model Based Controller

The goal is to design a controller that can robustly stabilize the RWM and meet specified controller performance criteria. The robust stability of the plant is determined by the N_{11} sub-matrix, where $N = F_l(P,K)$ represents the nominal closed-loop system. The sub-system N_{11} term isolates the uncertainty from the input and output of the system. The robust stability is determined by the structured singular value, which is defined as

$$\mu(N_{11}) \triangleq \frac{1}{min\{k_m | det(I - k_m N_{11}\Delta) = 0\}}$$

for $\bar{\sigma}(\Delta) \leq 1$. Larger μ values means $(I - N_{11}\Delta)$ becomes singular with small perturbations, thus the smaller μ the better. The robust stability condition is found by finding the smallest value of k_m at the onset of instability, or $det(I - k_m N_{11}\Delta) = 0$, which yields $k_m = \frac{1}{\mu(N_{11})}$, where k_m is a measure of the robust stability to perturbations in Δ. Thus, assuming N_{11} and Δ are stable, the system is robustly stable if and only if $\mu(N_{11}(j\omega)) < 1, \forall\omega$. Similarly, the robust performance is given by $\mu(N(j\omega)) < 1, \forall\omega$. Both conditions assume that N is internally stable.

DK-iteration is one available procedure to design a controller using μ-synthesis. Since there is no direct method to synthesize a μ-optimal controller, this method is used by combining $\mathscr{H}_\infty$ synthesis and μ-analysis. This method starts with the upper bound on μ in terms of the scaled singular value

$$\mu(N) \leq \min_{D \in \mathscr{D}} \bar{\sigma}\left(DND^{-1}\right)$$

where $\mathscr{D}$ is the set of matrices D which commute with Δ, i.e., $D\Delta = \Delta D$. Then, the controller that minimizes the peak value over frequency of this upper bound is found, namely

$$\min_K \left(\min_{D \in \mathscr{D}} \|DN(K)D^{-1}\|_\infty \right).$$

The controller is designed by alternating between the two minimization problems until reasonable performance is achieved. The DK-iteration can summarized as follows (Skogestad [2005]):
1. *K*-**step**. Synthesize an $\mathscr{H}_\infty$ controller for the scaled problem, $\min_K |DN(K)D^{-1}|_\infty$ with fixed D(s).
2. *D*-**step**. Find D($j\omega$) to minimize $\bar{\sigma}\left(DND^{-1}(j\omega)\right)$ at each frequency with fixed N.
3. Fit the magnitude of each element of D($j\omega$) to a stable and minimum-phase transfer function D(s) and go to step 1.
The iteration continues until $||DN(K)D^{-1}||_\infty < 1$ or the $\mathscr{H}_\infty$ norm no longer decreases.

Using the derived $P - \Delta$ formulation (Fig. 9), a controller can be designed with the *DK*-iteration method for robust stabilization. For the model being used the growth rate γ ranges from 10 rad/s to 5,000 rad/s. This results in a range for the uncertain parameter c_{pp} that goes from 71 to 0.3325. This is the range of values for which the system should be stabilized so that the robust controller can be considered a suitable design.

The complete system that is used to design the controller has an additional two time delay blocks preceding the plasma model. The time delays physically represent the plasma control system and the power supply. For design purposes, the time delays are linearized using second order Padé approximations.

Table 1. Performance Targets and Constraints.

Condition	Target Value	Maximum Constraint
Rise Time	1.0ms	5.0ms
Settling Time	5.0ms	10ms
Overshoot	15%	50%
Input Voltage	N/A	± 100V

Two controllers are synthesized using the *dksyn* ccommand in Matlab, one using the nominal plant and the other an augmented plant with input weight. The performance weight is added to the inputs of the system to achieve desired loop-shaping results. The weight is of the form $W = \frac{(M^{-1/n}s+\omega_b^*)^n}{(s+\omega_b^* A^{1/n})^n}$, where $M = 10^6$, $\omega_b^* = 10^9$, $A = 1$, and $n = 2$. The DK controllers are synthesized using a $P-\Delta$ system constructed for $c_{pp}^* = 0.34125$ ($\gamma^* = 4,890 rad/s$) and guarantees $\mu < 1$ for the range defined by $c_{pp_{min}} = 0.3325$, $c_{pp_{max}} = 0.35$, which is equivalent to $\gamma_{max} = 5,000 rad/s$, $\gamma_{min} = 4,660 rad/s$. However, these results are conservative and, as it will be shown in the next part, the stability and performance ranges for our system are indeed bigger. The conservatism is explained by the fact that the DK-iteration implicitly assumes that the uncertain parameter is complex and does not take advantage of the known phase information of the real uncertainty. The real uncertainty can be considered using a modified algorithm, the DGK-iteration (Young [1993]), however this algorithm greatly increases the numerical complexity. The controllers were designed using a 15 eigenmode model with 36 states. The designed controllers have orders of 108 and 107 for the plant without weight and with weight respectively. In both cases, the controller order is reduced to 16 before computing the effective stability and performance ranges.

4.2 Controller Simulation and Results

In order to be able to compare the proposed model-based DK controllers with present non-model-based controllers, a proportional-derivative (PD) controller is designed (integral action is not required for this system). The PD controller is synthesized to maximize the stability range as a function of γ and is of the form $K_{ij} = \frac{G_{P_{ij}} + G_{D_{ij}} s}{1+\tau_{pcs} s}$, for $i = 1 \ldots 3$, $j = 1 \ldots 2$, and with $\tau_{pcs} = 4 \times 10^{-4}$ sec. The resulting non-zero gains are $G_{P_{11}} = 3.80 \times 10^4$, $G_{D_{11}} = 76$, $G_{P_{22}} = 1.38 \times 10^4$, $G_{D_{22}} = 40$, $G_{P_{32}} = 6.62 \times 10^4$, $G_{D_{32}} = 103$. Table 1 provides the performance constraints in response to a unit step in the RWM mode amplitude.

Fig. 10 shows the time response to a unit step in the RWM mode amplitude at constant RWM growth rates of $\gamma = 10$ rad/s and $\gamma = 5,000$ rad/s, the lower and upper limits of the growth rate range of our interest. For the slower growth rate (top graph), the DK and PD controllers have similar responses with approximately 20% overshoot, and a fast rise and settling time. For the faster growth rate (bottom graph), the settling time is increased to approximately 5 ms. Another example is presented in Fig. 11, which shows the response to initial conditions of the plasma, normalized to a starting RWM mode amplitude of 1 Gauss. The DK controllers provide quick suppression of the RWM mode amplitude, out-performing the PD controller, which does not provide quick suppression at the faster growth rate. While the settling time is similar for both DK controllers, the weighted version slightly out-performs the non-weighted one. For both growth rates, the weighted DK controller design uses less applied voltage to achieve similar results.

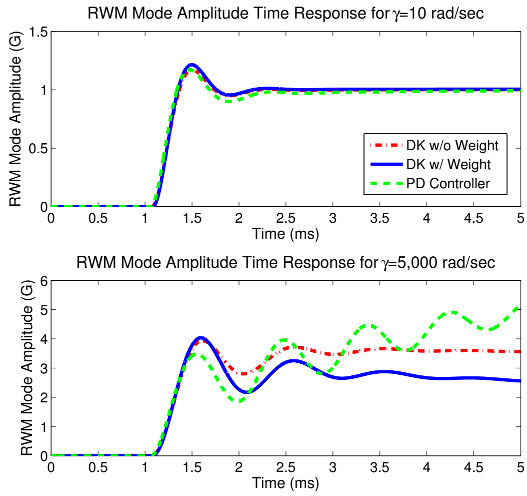

Fig. 10. Step response RWM mode amplitude for $\gamma = 10$ rad/s (top) and $\gamma = 5,000$ rad/s (bottom).

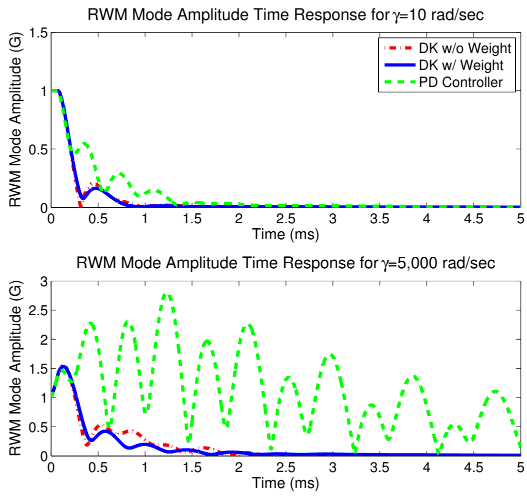

Fig. 11. Initial condition response RWM mode amplitude for $\gamma = 10$ rad/s (top) and $\gamma = 5,000$ rad/s (bottom).

Table 2. γ Stability and Performance Ranges.

Controller	*DK* w/o Weight	*DK* w/ Weight	*PD*
Stability Range	0 - 7,437 rad/s	0 - 8,434 rad/s	0 - 5,042 rad/s
Perf. Range (Step)	0 - 7,254 rad/s	0 - 7,450 rad/s	0 - 2,247 rad/s
Perf. Range (Initial)	0 - 6,459 rad/s	0 - 7,150 rad/s	0 - 5,980 rad/s

4.3 Closed-loop Stability and Performance

Table 2 provides the ranges of γ for which stability and performance conditions are satisfied. The first row *Stability Range* indicates the range of γ for which the system remains stable when using a unit step input for the RWM model amplitude. The second row *Perf. Range (Step)* represents the range of γ for which the performance conditions are satisfied under the same control input. The final row *Perf. Range (Initial)* indicates the range of γ for which the performance conditions are satisfied when an initial unit excitation of the RWM mode amplitude is forced through appropriate initial conditions. Both model-based DK controllers show good stability and performance properties well beyond the desired γ range and that of the PD controller, with the weighted DK controller design having a larger range in both stability and performance.

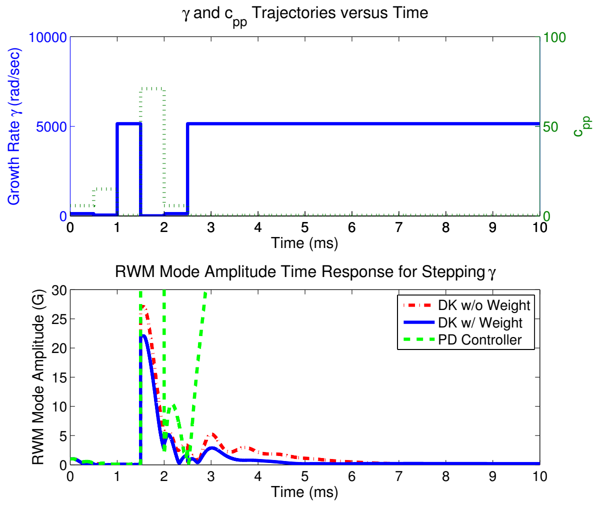

Fig. 12. Initial condition response control inputs for stepping γ with *DK* controller.

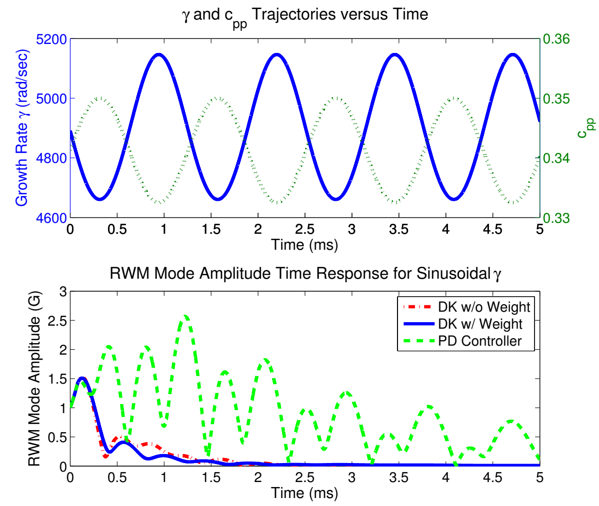

Fig. 13. Initial condition response control inputs for sinusoidal γ with *DK* controller.

Since the robust controller stabilizes the plant over a range of growth rate, it is of interest to investigate the controller performance using time-varying of growth rate γ. The results for stepping, and sinusoidal excitation of the c_{pp} parameter are presented (Fig. 12- 13). The step function also initiates at $c_{pp} = 5.75$ and changes between the maximum, nominal, and minimum values of c_{pp} in 0.5 ms intervals over a 2.5 ms span. The amplitude of the sinusoidal function is defined by the design range of c_{pp} used for the synthesis of the controller. Its frequency is 5,000 rad/sec. In both cases, the RWM mode amplitude is quickly suppressed (Fig. 12- 13). Again, the weighted *DK* controller design maintains less RWM amplitude compared to the nominal *DK* controller, providing better rejection to changes in the growth rate. In all cases the *PD* controller has difficulty suppressing the RWM amplitude and becomes unstable in the stepping c_{pp} case.

5. CONCLUSIONS

The GA/Far-Tech DIII-D RWM model was restructured into a robust control framework, isolating the RWM time-varying uncertain parameter c_{pp}, the key term influencing the size of the RWM instability. With the system model in this framework, the *DK*-iteration method was applied to develop robust controllers, as measured by the structured singular value, for a predetermined range of γ. Augmenting the nominal system with performance weight provides better loop-shaping of the closed-loop system, which results in improved controller performance. Since the plasma RWM growth rate can vary with operating conditions, the design of a controller that can stabilize the system over the entire physical range of γ is critical. In terms of robust stability, this method eliminates the need of online identification and controller scheduling.

REFERENCES

Edgell D.H., Kim J.S., *et al.*, "Magnetohydrodynamic mode identification from magnetic probe signals via a matched filter method," *Rev. Sci. Instrum.*, v 73, n 4, April 2002, p 1761.

Fransson C.M. , Edgell D.H. , Humphreys D.A. and Walker M.L., "Model validation, dynamic edge localized mode discrimination, and high confidence resistive wall mode control in DIII-D," *Phys. Plasmas*, v 10, n 10, October 2003, p 3961.

Garafalo A.M., *et al*, "Resistive wall mode dynamics and active feedback control in DIII-D," *Nucl. Fusion*, v 41, n 9, September 2001, p 1171.

In Y., *et al*,"Model-based dynamic resistive wall mode identification and feedback control in the DIII-D tokamak," *Phys. Plasmas*, v 13, n 6, June 2006, p 62512-1-12.

Kailath T., *Linear Systems*, Prentice-Hall, 1979.

Katsuro-Hopkins O., *et al*, "Enhanced ITER resistive wall mode feedback performance using optimal control techniques," *Nucl. Fusion*, v 47, n 9, Sep 1, 2007, p 1157-1165.

Okabayashi M., *et al*, "Active feedback stabilization of the resistive wall mode on the DIII-D device," *Phys. Plasmas*, v 8, n 5 II, May 2001, p 2071.

Okabayashi M., *et al*, "Control of the resistive wall mode with internal coils in the DIII-D tokamak," *Nucl. Fusion*, v 45, n 12, December 2005, p 1715-31.

Packard A.K., *What's new with μ: Structured uncertainty in multivariable control*, Ph.D. Thesis, University of California at Berkeley, 1988.

Pironti A. and Walker M.L.,"Fusion, Tokamaks, and Plasma Control," *IEEE Control Systems Magazine*, v 25, n 5, October 2005, p.30-43.

Sen A.K., *et al*, "Optimal control of tokamak resistive wall modes in the presence of noise," *Phys. Plasmas*, v 10, n 11, November 2003, p 4350.

Skogestad S. and Postlethwaite I., *Multivariable Feedback Control; Analysis and Design*, Wiley, 2005.

Sun Z., *et al*, "Adaptive optimal stochastic state feedback control of resistive wall modes in tokamaks," *Phys. Plasmas*, v 13, n 1, January 2006, p 012512.

Strait E.J., *et al*, "Resistive wall mode stabilization with internal feedback coils in DIII-D," *Phys. Plasmas*, v 11, n 5 II, May 2004, p 2505.

Walker M.L., Humphreys D.A., *et al.*, "Emerging Applications in Tokamak Plasma Control," *IEEE Control Systems Magazine*, v 26, n 2, April 2006, p.35-61.

Wesson J., *Tokamaks*, Clarendon Press, Oxford, 3rd ed., 2004.

Young P.M., *Controller Design with Real Parametric Uncertainty*, Technical Memorandum No. CIT-CDS 93-016, California Institute of Technology, 1993.

Zhou K., Doyle J.C., and Glover K., *Robust and Optimal Control*, Prentice Hall, 1996.